Climate Resilience and Sustainability

WILEY | RMetS Royal Meteorological Society

ORIGINAL ARTICLE OPEN ACCESS

A Framework for Quantifying Diverse Multi-Hazard Interactions to Enhance Climate Resilience

Mohammed Sarfaraz Gani Adnan[1] | Christopher J. White[2] | Eleonora Perugini[3] | Esther Hlíðar Jensen[4] | Talfan Barnie[4] | Natalia Castillo[5] | Marcello Arosio[5] | Enrico Tubaldi[2] | Matthew James Roberts[4] | Marco Gaetani[5] | Younghwa Cha[6] | Frederiek Sperna Weiland[7] | Mario Martinelli[8] | John Douglas[9]

[1]Department of Civil and Environmental Engineering, Brunel University of London, Uxbridge, UK | [2]Department of Civil and Environmental Engineering, University of Strathclyde, Glasgow, UK | [3]Department of Civil, Environmental and Mechanical Engineering, University of Trento, Trento, Italy | [4]Icelandic Meteorological Office, Reykjavík, Iceland | [5]Scuola Universitaria Superiore IUSS, Palazzo del Broletto, Pavia, Italy | [6]Global Research Institutes, The Lyell Centre, Heriot-Watt University, Edinburgh, UK | [7]Department of Inland Water Systems, Deltares, Delft, the Netherlands | [8]SPERI S.p.A, Rome, Italy | [9]Frazer-Nash Consultancy, Glasgow, UK

Correspondence: Mohammed Sarfaraz Gani Adnan (sarfaraz.adnan@brunel.ac.uk)

Received: 19 June 2025 | **Revised:** 29 March 2026 | **Accepted:** 24 August 2026

Keywords: climate change | Europe | extreme events | joint probability | multi-hazard interaction

ABSTRACT

Multi-hazard events generate impacts exceeding those of individual hazards but remain difficult to assess due to complex interactions. This study presents a generalized framework for analyzing four interaction types—multivariate, preconditioned and triggering, spatially, and temporally compounding events—across current and future climates. Combining extreme-event detection, Bayesian copula modeling, and spatial analysis, the framework enables consistent multi-hazard characterization beyond pairwise approaches. Applications to four European case studies reveal strong hazard dependencies and increased multi-hazard occurrence under future climate scenarios.

1 | Introduction

In recent years, multi-hazard events have gained increasing attention from governmental and international organizations due to their growing threats to human lives, infrastructure, and economic systems (Gill and Malamud 2014; Lee et al. 2024; Zscheischler et al. 2020). These events involve complex and often nonlinear interactions among hazards that may occur simultaneously, sequentially, or through cascading processes across space and time. Their impacts are frequently shaped by interrelated physical, ecological, and socioeconomic drivers, making the resulting consequences substantially greater than the sum of individual hazards (Zscheischler et al. 2020). As climate variability, urbanization, and environmental change intensify hazard exposure and vulnerability worldwide, the need for robust approaches to understanding and assessing multi-hazard interactions has become increasingly urgent.

Previous studies have identified several major categories of multi-hazard interactions. Common categories include compound (Zscheischler et al. 2020), consecutive (De Ruiter et al. 2020), triggering (Gill and Malamud 2014), and amplifying (Gill et al. 2020) hazards, each describing different forms of temporal, spatial, or causal relationships between events. A widely adopted framework further distinguishes four types of compound interactions: multivariate, preconditioned, spatially compounding, and temporally compounding (Zscheischler et al. 2020). More recent refinements include geophysical hazards and further distinctions in triggering mechanisms (Lee et al. 2024).

A wide range of qualitative, quantitative, and hybrid methods has been developed to analyze multi-hazard interactions (Ciurean et al. 2018; Kennedy et al. 2023; Tilloy et al. 2019). Qualitative or semiquantitative methods—such as narrative descriptions of historical events (Ciurean et al. 2018), hazard wheels (Rosendahl Appelquist and Halsnæs 2015), hazard matrices (Gill and Malamud 2014), hazard maps (Johnson et al. 2016), and network diagrams (van Westen 2012)—are commonly used to identify potential relationships between hazards and to support exploratory assessments where empirical data are limited. Quantitative approaches include physical process-based models or systems-based approaches (Chen et al. 2016; Fan et al. 2020; Gnyawali et al. 2023) and probabilistic and statistical analyses that estimate joint probabilities, cascading effects, or interaction intensities (Boult et al. 2022; De Angeli et al. 2022; Domeisen et al. 2023; Han et al. 2019; Wang et al. 2013; Wu et al. 2022). Hybrid approaches combine elements of both methodologies, integrating statistical or probabilistic frameworks with process-based or climate models to incorporate observational data alongside simulated scenarios (Ming et al. 2022; Pourghasemi et al. 2020; Tanim and Goharian 2021; Thompson et al. 2017). Despite these advances, each methodological family presents limitations: Qualitative approaches typically lack the ability to quantify impacts or probabilities (van Westen and Greiving 2017), whereas quantitative models often require extensive data, high computational resources, and detailed process understanding (Kennedy et al. 2023; Tilloy et al. 2019).

Assessing multi-hazard interactions is further complicated by the diversity of hazard types, the wide range of temporal and spatial scales involved, and the interdisciplinary nature of the analyses. Differences in measurement units, event magnitudes, and probability structures make it difficult to harmonize datasets and compare interaction effects across hazards. Moreover, ambiguities in the definitions and typologies of multi-hazard events continue to create inconsistencies in methodological applications and reporting practices (Gill et al. 2022; Hochrainer-Stigler et al. 2023; Ward et al. 2022). Analyzing multi-hazard risk cannot be reduced to a simple aggregation of individual hazards—a concept sometimes described as a "multi-layer single-hazard" approach—because interactions between hazards may produce nonlinear amplification, cascading failures, or feedback mechanisms that significantly alter expected impacts (Gill and Malamud 2016). The absence of a widely adopted, generalized framework capable of systematically capturing these diverse interaction processes remains a major challenge for effective multi-hazard risk assessment and management (Ward et al. 2022). Additional barriers include the limited availability of comprehensive multi-hazard datasets and the ongoing difficulty of translating scientific knowledge on hazard interactions into operational policy and decision-making contexts (Trogrlić et al. 2024).

Empirical research on multi-hazard interactions has expanded substantially in recent years, yet most studies have concentrated on examining the joint occurrence of multiple events (Bevacqua et al. 2019, 2021; Claassen et al. 2023; De Angeli et al. 2022; Leonard et al. 2014; Moftakhari et al. 2017; Wahl et al. 2015; Zscheischler and Seneviratne 2017). Typical examples include compound coastal and fluvial flooding (Bevacqua et al. 2019; Ghanbari et al. 2021; Ming et al. 2022; Wahl et al. 2015; Moftakhari et al. 2017), concurrent wind and precipitation extremes (Bloomfield et al. 2024), combined heat and drought events (Zscheischler and Seneviratne 2017), and combined surge and precipitation events (van den Hurk et al. 2015). Although these investigations have provided important insights into joint probabilities, impact amplification, and modeling techniques, their focus on hazard pairs limits the capacity to examine more complex interaction structures involving multiple hazards, cascading sequences, or combinations of different interaction mechanisms (Zscheischler et al. 2020). More recently, Bevacqua et al. (2021) presented guidelines for studying four types of compound weather and climate events (e.g., multivariate, preconditioned, spatially compounding, and temporally compounding events). However, the methodological guidelines for these events tend to demonstrate analytical procedures using specific hazard pairs, leaving limited guidance for extending these methods to broader multi-hazard systems involving multiple interacting drivers.

To address these limitations, there remains a need for a comprehensive analytical framework capable of systematically examining different categories of multi-hazard interactions within a unified structure and extending beyond joint occurrence of multiple hazards. Building on established compound-event typologies (Lee et al. 2024; Zscheischler et al. 2020) and guidelines (Bevacqua et al. 2021; Jensen et al. 2024), this study introduces a generalized framework for investigating multivariate, preconditioned and triggering, spatially compounding, and temporally compounding interactions under both present-day and future climate conditions. The framework aims to enable more consistent quantification of interaction effects, facilitate comparisons across hazard types and regions, and support improved integration of multi-hazard considerations into risk assessment and disaster risk management practices.

2 | Materials and Methods

2.1 | Framework to Quantify Multi-Hazard Interactions

This section presents a generalized framework to analyze four types of multi-hazard events. For specific hazard types, the framework is constructed by examining the spatial and/or temporal patterns of interactions between two individual hazards. The proposed framework builds upon the approaches presented in Jensen et al. (2024) and visually summarized in Figure 1.

2.1.1 | Multivariate Events

Multivariate events are defined as "the co-occurrence of multiple climactic drivers and/or hazards in the same geographical region causing an impact" (Zscheischler et al. 2020). To analyze multivariate events, the study adopts a bivariate hazard assessment framework commonly used in compound-event research (Bateni et al. 2022; Ghanbari et al. 2021; Latif and Mustafa 2020), enabling quantification of joint probabilities and interactions between paired hazards. The workflow (Figure 1) comprises three steps: identifying joint extreme events, estimating their marginal and joint return periods (JRPs), and generating intensity maps for single and compound hazard scenarios.

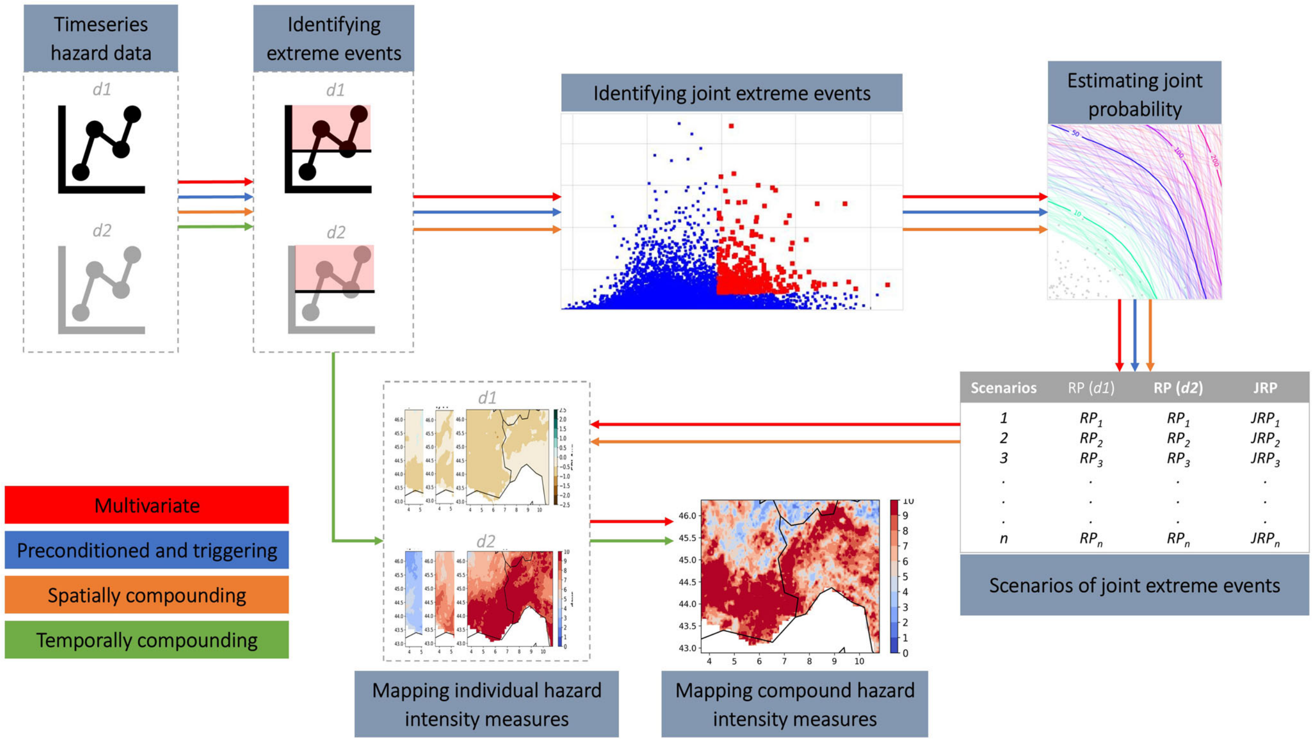

FIGURE 1 | Conceptual framework for multi-hazard event analysis. The diagram illustrates the proposed framework for analyzing four types of multi-hazard interactions. Colors of boxes and connecting lines indicate different interaction types. d_1 and d_2 represent two interacting hazards.

Joint extreme events are first identified by selecting time series of hazard intensity measures (e.g., d_1 and d_2) from the same region and harmonizing them through preprocessing (e.g., anomaly removal, resampling, and overlapping-period filtering). This selection of data points is based on measurement type, temporal resolution, and spatial proximity of data points. Extreme values are extracted using a threshold-excess method, supported by quantile regression to define suitable thresholds that balance extremity with data availability (Ming et al. 2022). Dependency between hazards is assessed using Kendall's rank correlation coefficient (τ), and compound events are determined when exceedances occur simultaneously or within a short temporal window (typically 3–7 days (Salvadori et al. 2016)). Only the maximum paired intensities within each window are retained for further analysis. A MATLAB toolbox (*detectExtremeEvents*) is developed to automate this procedure and generate joint-event time series (see Data Availability Statement).

Following detection of joint extremes, their marginal return periods (MRPs) and JRPs are estimated (Brunner et al. 2016). MRPs are derived from the marginal exceedance probability $G_D(d)$, whereas JRPs are obtained from the joint exceedance probability $G_{D_1 D_2}(d_1, d_2)$; full details and equations are provided in the Supporting Information. Marginals are modeled using Generalized Pareto Distributions (GPD), and dependence is captured using a Gumbel copula (Gudendorf and Segers 2010), which is well suited for upper tail dependence typical of compound hazards (e.g., surge-rainfall extremes) (Gori et al. 2022; Ismail et al. 2018; Xi et al. 2023). Parameters for the marginal GPDs and copula are estimated using a Bayesian framework implemented in Stan (Carpenter et al. 2017). Posterior diagnostics—including $\hat{R}$, effective sample sizes, divergence checks, Bayesian Q–Q plots, and posterior predictive checks—ensure robust characterization of both marginal and joint behavior.

Finally, multivariate scenarios are generated by pairing sampled JRPs with their corresponding intensities (d_1, d_2), enabling exploration of different combinations of hazard severity. Numerical simulations use these intensity pairs to produce spatial hazard maps for individual and compound events, facilitating assessment of scenarios ranging from high-surge/low-flow, for instance, to concurrent high-intensity extremes.

2.1.2 | Preconditioned and Triggering Events

Preconditioned and triggering events occur when one hazard initiates or increases the likelihood of another, meaning a single primary driver may generate none, one, or multiple secondary hazards (Kennedy et al. 2023). In this study, meteorological or climatological conditions act as preconditions that may trigger geophysical hazards, such as heavy rainfall inducing landslides. Identifying these relationships begins by detecting peaks in the hazard intensity time series. For hillslope-scale analyses, time series segmentation is performed using a peaks-over-threshold (POT) approach, which selects independent exceedances separated by several days (typically 3–7) to ensure event independence. Consistent with the Pickands–Balkema–De Haan theorem (Balkema and De Haan 1974; Pickands III 1975), exceedances above the chosen threshold follow a GPD defined by location, scale, and shape parameters, where the threshold serves as the location parameter (Park and Kim 2016).

Joint preconditioned–triggered events are identified using a procedure analogous to the multivariate analysis (Section 2.1.1). Extreme events are first detected independently in both time series using POT without separating dependent peaks. For each extreme preconditioned event, a search window—typically 3–7 days—is defined to identify any corresponding triggered event. The window length and threshold choice are guided by Kendall's τ to ensure both meaningful dependence and event independence. If at least one extreme triggered event occurs within the window, the pair is classified as a triggering relationship, and only the maximum triggered intensity is retained. Preconditioned events that do not lead to an extreme triggered response are excluded from subsequent probability estimation.

Once joint peaks are identified, their return periods are computed using the same copula-based Bayesian framework implemented in Stan (Section 2.1.1), enabling estimation of the dependence structure and associated uncertainty.

2.1.3 | Spatially Compounding Events

Spatially compounding events occur when multiple connected locations experience the same or different hazards within a limited time window, jointly contributing to impacts (Zscheischler et al. 2020). To identify such events, gridded time series of hazard intensity measures are processed by extracting, at each time step, the maximum value of each hazard across all grid cells within the study area. This produces two spatially aggregated time series—one for each hazard—on which joint extreme events are identified following the procedure described in Section 2.1.1.

Using these joint extremes, JRPs are estimated through the same copula-based approach employed for multivariate analysis (Section 2.1.1). The resulting JRPs are combined with their corresponding intensity pairs to generate scenarios representing different severities of spatially compounding events, enabling assessment of potential multi-hazard interactions across the study region.

To evaluate the spatial structure and magnitude of these events, hazard intensity maps are constructed for selected RPs. Extreme value analysis (EVA) is applied independently to each grid cell using the block maxima method, whereby annual (or relevant temporal) maxima are extracted to form an annual maxima series (AMS). Under classical extreme value theory, AMS values follow a generalized extreme value (GEV) distribution defined by location, scale, and shape parameters (Coles et al. 2001; Gilleland and Katz 2016). Once fitted, the GEV model is used to estimate return periods for each grid cell, allowing spatial comparison of hazard intensities under individual- or compound-event scenarios.

2.1.4 | Temporally Compounding Events

Temporally compounding events involve sequences of hazards affecting the same region within a defined period, where their combined occurrence amplifies impacts relative to isolated events (Zscheischler et al. 2020). These sequences may consist of successive climate extremes or multiple moderate anomalies that interact to intensify system-level consequences (Liu et al. 2016; Tilloy et al. 2019; Zscheischler et al. 2020). Figure 1 outlines the steps used to quantify temporally compounding events based on pairs of interacting hazards.

The analysis begins by identifying each hazard individually using appropriate indices derived from standardized indicators or percentile-based thresholds. Different hazards require different temporal resolutions; for example, heatwaves in this study are defined using daily maximum temperatures exceeding the 90th percentile for at least three consecutive days (Perkins and Alexander 2013; Rousi et al. 2022), and longer term conditions are captured using monthly standardized indices. A range of indicators can be applied depending on study objectives. Here, heatwaves are detected using a monthly Standardized Heatwave Index (HWI), whereas droughts are identified using the 3-month Standardized Precipitation Index (SPI-3), suitable for diagnosing sustained precipitation deficits (Hao et al. 2014; McKee et al. 1993).

Compound co-occurrence is assessed over extended periods—typically monthly—where both individual hazards occur within the same interval. Unlike short-term compound-event analyses that evaluate dependence over 1–7 day windows (Liu et al. 2015; Ming et al. 2015, 2022), this approach captures broader patterns of co-occurrence without estimating joint probabilities. Compound events are identified separately at each grid cell, and results are stored in annual matrices, enabling spatially explicit analysis across the study area. The relevant timescale of co-occurrence varies by hazard type; for example, droughts develop over weeks to months, whereas other hazards may emerge over shorter or longer periods.

Mapping individual and temporally compounding events involves summarizing and visualizing hazard occurrence across the selected timescales. Initial maps depict the spatial distribution and frequency of each hazard, followed by maps showing the frequency of their combined occurrence at seasonal or monthly scales. This spatial–temporal representation highlights regions experiencing repeated or persistent compound risks and provides valuable insights for impact assessment, planning, and risk mitigation.

2.2 | Application of the Generalized Multi-Hazard Framework

2.2.1 | Selecting Multi-Hazard Events in Case Study Areas

The generalized multi-hazard interaction framework presented in Section 2.1 is applied to four case study regions—Oslo (Norway), Múlaþing (Iceland), Essex (UK), and Nice (France)—as part of the Multi-hazard and Risk-informed System for Enhanced Local and Regional Disaster Risk Management (MEDiate) project (https://cordis.europa.eu/project/id/101074075). For each region, one representative pair of interacting hazards was selected for detailed analysis (Figure 2). The selection process followed a Participatory Action Research (PAR) approach (Komendantova et al. 2023), in which local stakeholders played an active role in identifying and prioritizing the hazard interactions most relevant to their regional risk contexts.

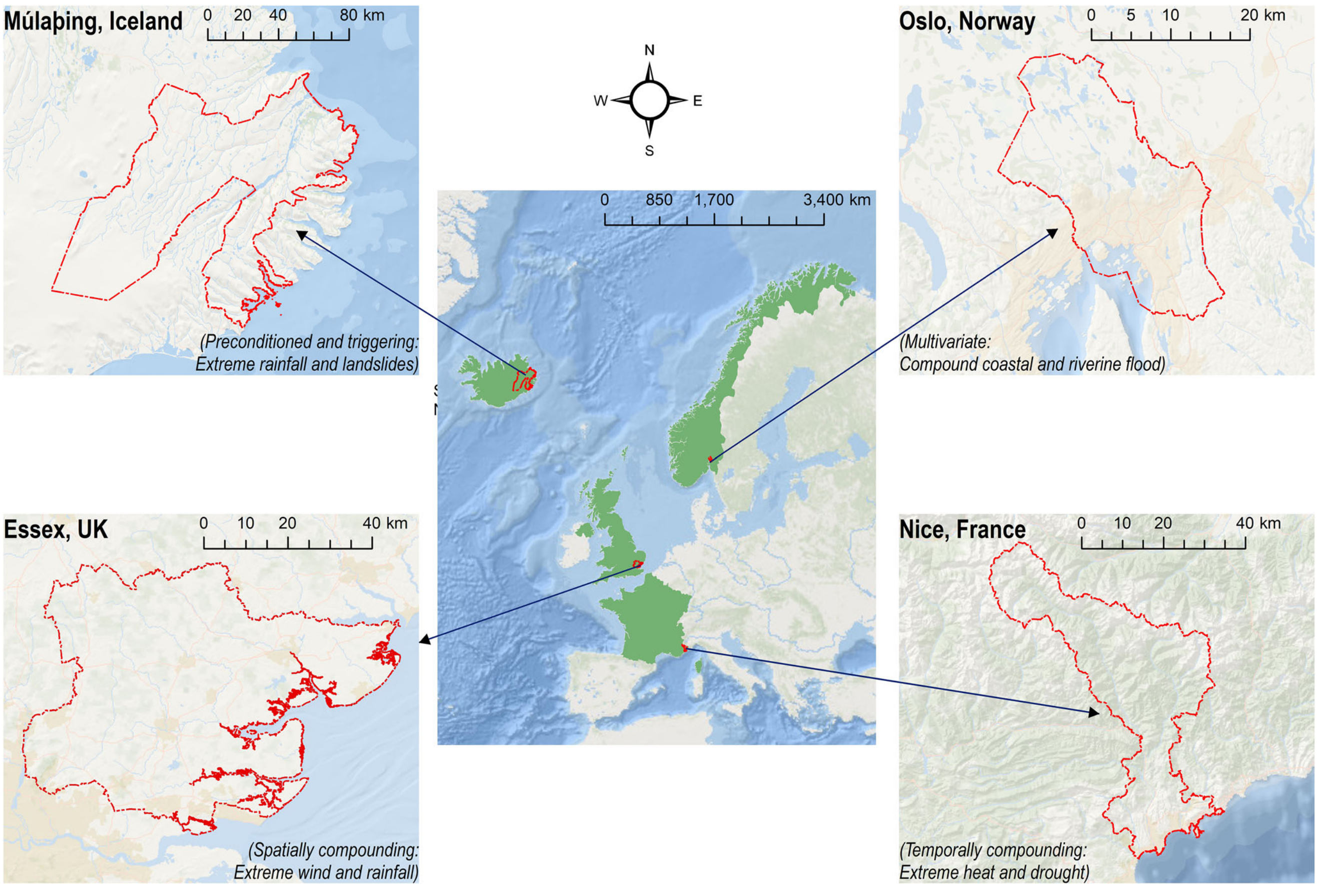

FIGURE 2 | Case study regions and associated multi-hazard interactions. Map showing the four study regions where the framework is applied, together with the corresponding hazard combinations and interaction types analyzed in each location.

A project-wide PAR workshop held in June 2023 brought together stakeholders from all four regions to explore multi-hazard dynamics, including situations where hazards co-occur, trigger secondary processes, or lead to cascading impacts. Participants were introduced to a structured typology of multi-hazard interactions comprising four categories: multivariate, preconditioned and triggering, spatially compounding, and temporally compounding events. This typology provided a consistent framework for evaluating how different hazard combinations may interact to intensify impacts. Through guided discussion and regional breakout sessions, stakeholders identified and ranked the hazard interactions of greatest concern in their respective regions. From these prioritized lists, three key hazard pairs per region were proposed, from which one representative pair per case study was selected for implementation and testing of the multi-hazard interaction framework.

2.2.2 | Case Study 1: Multivariate Events in Oslo, Norway

The multivariate framework is applied to Oslo to assess compound coastal–riverine flood events using surge height (m) and river flow (m^3/s) as the hazard intensity measures. Oslo covers 454 km^2, with approximately 650,000 inhabitants, and its geographical setting makes it susceptible to both riverine flooding and storm surge impacts (IPCC 2013). A notable historical example occurred in October 1987, when prolonged heavy rainfall—reaching 240% of normal levels over a 30-day period—coincided with spring tides and strong winds. This overlap produced flood conditions with recurrence intervals approaching 100 years and resulted in damages exceeding 650 million NOK (~€147 million), surpassing the combined national natural disaster compensation of the previous 4 years (Engen 1988).

Due to the lack of high-resolution future river-flow projections, the compound flood analysis relies entirely on observational datasets. Compound flood events in Oslo are identified between 1967 and 2023. Surge records are obtained from Oslo's only tidal gauge operated by the Norwegian Hydrographic Service, whereas river flow observations are taken from the Gryta station, located approximately 10 km upstream and operated by NVE Sildre (Figure S2, Table 1). Compound flood events are identified when both variables exceed their respective thresholds, and a sensitivity analysis is conducted to test different percentile thresholds for event detection (Figure S3).

JRPs are estimated using the Stan-based copula framework described in Section 2.1.1, applying GPDs to model the marginal distributions of surge and river flow under uniform priors. Four Markov chains of 5000 samples each demonstrate strong convergence, with effective sample sizes and $\hat{R}$ values confirming stable posterior sampling. Bayesian Q–Q plots indicate good marginal GPD performance for moderate extremes, with expected reductions in fit for the largest observed values. Additional diagnostics,

TABLE 1 | Data used for analyzing multi-hazard interactions.

Case study	Multi-hazard interactions	Indicator	Timeframe	Temporal resolution	Spatial resolution	Source
Oslo	Compound flood	Surge height (m)	October 1967–July 2023	Hourly	Station data	Norwegian Centre for Climate Services (https://seklima.met.no/observations/)
		River flow (m^3/s)	October 1967–July 2023	Hourly	Station data	
		Depth (m) and extent (m^2) of riverine flooding	Base year: 1980 Projected year: 2030, 2050, 2080	Return periods: 1, 2, 5, 10, 25, 50, 100, 250, 500, and 1000 years	$5' \times 5'$	Aqueduct Floods Hazard Maps (Ward et al. 2020)
		Depth (m) and extent (m^2) of coastal flooding	Base year: 2017 Future year: 2100	Return periods: 20, 200, and 1000 years	Vector data	The Norwegian Water Resources and Energy Directorate—NVE (https://temakart.nve.no/)
Múlaþing	Extreme rainfall and landslide	Rainfall (mm)	1980–2016	Hourly	2.5 km × 2.5 km	Icelandic reanalysis atmospheric (ICRA) project (Nawri et al. 2017)
		Projected rainfall (mm)	2020–2099	Hourly	2.5 km × 2.5 km	
		Landslide inventory (frequency)	1981–2015	Daily	Vector data	Icelandic Meteorological Office (https://en.vedur.is/)
Essex	Spatially compounding	Near-surface wind speed (m/s)	1980–2080	Daily	12 km	EuroCORDEX-UK: Regional climate projections for the UK domain (Barnes 2023)
		Rainfall (mm)				
Nice	Temporally compounding events	2-m temperature (°C)	1971–2100	Daily	5 km	EuroCORDEX: Regional climate simulations, downscaled, and bias corrected (Berg et al. 2021)
		Rainfall (mm)				

Note: Overview of the datasets used for the four multi-hazard case studies, including data types, variables, and their role in the framework application.

including posterior predictive checks and dependence-structure assessments, are provided in Figures S4–S7.

To explore potential spatial impacts, the study incorporates secondary inundation datasets. Riverine flood extents are derived from Aqueduct Global Flood Maps (Ward et al. 2020), whereas coastal flood extents are obtained from national flood maps (NVE 2023). Vector coastal datasets are converted to gridded raster layers following Cohen et al. (2018), using the European Digital Elevation Model (EU-DEM) at 25 m resolution.

2.2.3 | Case Study 2: Preconditioned and Triggering Events in Múlaþing, Iceland

This case study examines preconditioned and triggering relationships between extreme rainfall and landslides in the Múlaþing region of eastern Iceland, focusing on the town of Seyðisfjörður. The municipality covers 10,671 km^2 and has a population of 5359, including approximately 685 residents in Seyðisfjörður (2019). Steep mountainsides and highly variable topography, with elevations up to 1085 m, make the area particularly prone to snow avalanches and landslides (Arnalds et al. 2002). The region experienced a major landslide sequence in December 2020, when multiple debris flows culminated in a 74,000 m^3 slide causing widespread damage and evacuations, underscoring a long history of landslide risk that includes fatal events, such as the 1950 slide (Gylfadóttir et al. 2021; Jensen and Sönser 2003).

To analyze rainfall–landslide interactions, the antecedent precipitation index (API) is used as a proxy for relative soil moisture (Zhao et al. 2011). The API is calculated using a weighted sum of preceding daily rainfall (Cordery 1970; Li et al. 2021; Xie and Yang 2013), and this study applies a scaled normalized API (sNAPI) following established approaches (Ghosh et al. 2021; Heggen 2001). Rolling rainfall accumulations over 1-, 2-, 3-, and 5-day periods capture the short- and medium-term conditions relevant to slope instability. Hourly rainfall data are sourced from the ICRA project (Nawri et al. 2017) using the grid point nearest the Vestdalur station (~2.5 km from Seyðisfjörður), with model-observation consistency demonstrated by a strong correlation of 0.93 (Massad et al. 2020). The analysis uses 1980–2016 as the baseline period and 2030–2066 for future projections.

Joint extreme events—representing combinations of high rainfall and elevated sNAPI—are identified using the preconditioned–triggering methodology described in Section 2.1.2, and JRPs are subsequently estimated to characterize the likelihood of rainfall-driven landslide precursors.

2.2.4 | Case Study 3: Spatially Compounding Events in Essex, United Kingdom

Spatially compounding events in Essex are assessed by analyzing joint extreme wind and rainfall events. Essex, located in eastern England, is a predominantly low-lying county covering 3670 km^2 with an extensive 905 km coastline. Approximately 185,000 residents live across the region, with higher population densities concentrated along the southern coast. Its long coastline and interconnected river systems contribute to high exposure to storm surges and flooding (Spencer et al. 2015). The winter of 2013/2014 exemplified these risks, as a succession of intense Atlantic storms produced strong winds, heavy rainfall, and widespread coastal and fluvial flooding. A major storm surge on 5–6 December 2013 caused substantial damage, which was further exacerbated by additional storms in early January 2014 (Kendon and McCarthy 2015).

Daily maximum near-surface wind speed at 10 m (m/s) and daily rainfall (mm) are used as intensity measures. Data are separated into baseline (1981–2001) and future (2030–2050) periods. Following the methodology in Section 2.1.3, spatially aggregated daily maxima are calculated for each hazard across all grid points to construct time series for wind and rainfall. Joint extremes are identified when both variables exceed their respective thresholds, which are selected through a sensitivity analysis using baseline data. Threshold combinations are tested, and the pair producing the highest positive Kendall's τ is adopted (Table S4). The same thresholds are applied to the future dataset to ensure comparability across time periods.

JRPs are then estimated using the Stan-based copula model described earlier. Model diagnostics—including convergence assessments, posterior predictive checks, and dependence evaluations—are presented in Figures S11–S15, confirming the robustness of the joint-probability estimates.

2.2.5 | Case Study 4: Temporally Compounding Events in Nice, France

Temporally compounding events in Nice are analyzed through the co-occurrence of extreme heat and drought conditions. Nice lies within the Nice Côte d'Azur Metropolis in southeastern France, covering approximately 1500 km^2 and home to more than 540,000 residents. Its combination of coastal lowlands and steep mountainous terrain exposes the region to a wide range of natural hazards, including heatwaves, droughts, landslides, and coastal and riverine flooding. The Mediterranean climate has contributed to increasingly frequent and intense summer heatwaves and droughts, exemplified by the extreme summer of 2003 and prolonged drought episodes from 2004 to 2007 and in 2015 (Hauser et al. 2017; Rebetez et al. 2006).

Heat and drought conditions for the summer season (June–August) are quantified using the standardized HWI and the SPI3, respectively, based on daily temperature and precipitation data (Table 1). Data are derived from the CSC-REMO2009 regional climate model (REMO), downscaled from the MPI–ESM–LR global model for the historical period (1971–2005) and future projections (2006–2100) under RCP 8.5. Bias correction using Copernicus EFAS-Meteo datasets (Ntegeka et al. 2013) yields a 5-km spatial resolution.

Heatwave identification follows a two-stage process. First, heatwaves are defined as at least three consecutive days with maximum temperatures exceeding the 90th percentile, calculated using a 15-day moving climatological window (Fischer and Schär 2010). These daily events are then aggregated into a monthly standardized HWI, with values ≥1 classified as monthly heatwave events. Drought events are identified using SPI3 for June–August, computed via a nonparametric approach in which empirical precipitation probabilities are estimated using the Gringorten plotting position (Farahmand and AghaKouchak 2015; Gringorten 1963) and then transformed to standardized SPI values (Hao et al. 2014). The SPI3 represents precipitation totals accumulated over a 3-month window, including the respective and the 2 preceding months (e.g., August SPI3 corresponds to June–August). Summer months with SPI3 ≤ −1 are labeled drought events.

Temporally compounding heatwave–drought events are identified at each grid cell and month where both conditions co-occur (HWI ≥ 1 and SPI3 ≤ −1). These compound events are assessed across three 30-year periods—1976–2005, 2041–2070, and 2071–2100—to evaluate historical conditions and projected future changes in compound heat and drought risks.

3 | Results

3.1 | Compound Coastal and Riverine Flood Events in Oslo

Applying the multivariate framework to Oslo identifies the 95th percentile as the optimal threshold for both surge height and river flow, producing a Kendall's τ of 0.18. These thresholds correspond to 0.617 m for surge height and 0.706 m^3/s for river flow, yielding 41 compound flood events where both variables exceed their respective thresholds (Figure 3). These events represent instances of concurrent extreme coastal and riverine conditions.

Figure 4 illustrates the JRPs associated with these compound events. The upper right panel displays JRPs as a contour surface across combinations of surge height and river flow, whereas the lower left panel maps the MRP of the corresponding values. The remaining panels show the separate MRPs for each variable, supporting interpretation of individual and joint hazard contributions.

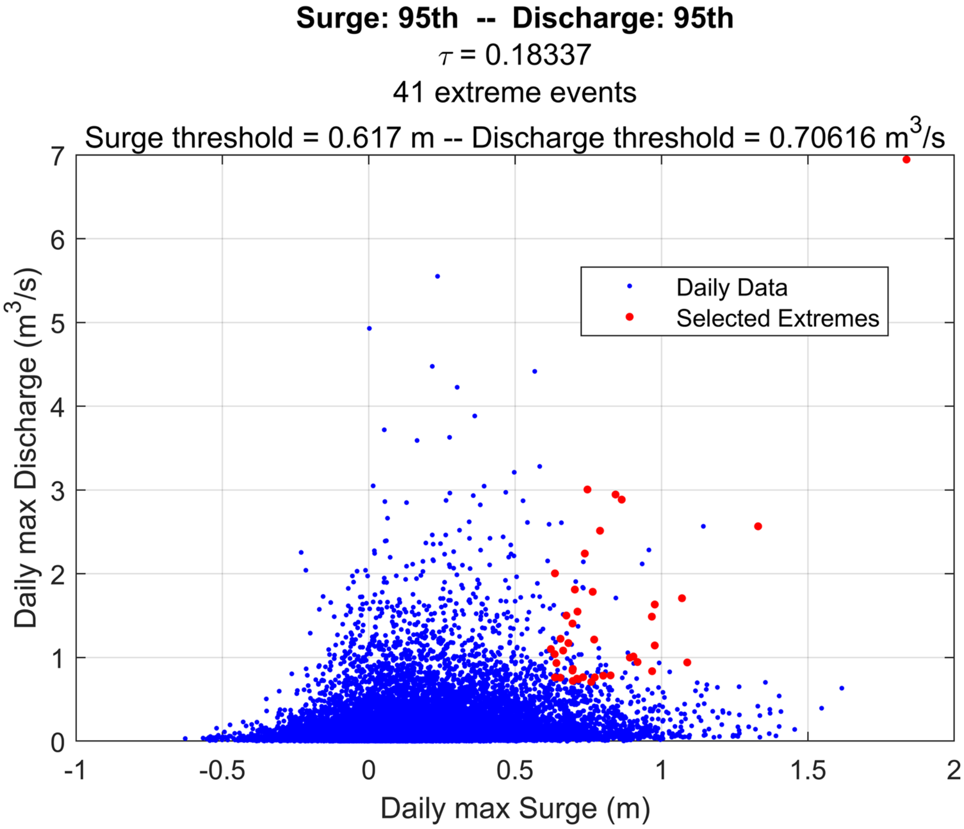

FIGURE 3 | Compound flood events in Oslo, Norway. Scatter plot of sea surge levels and river flow. Blue points represent all observed pairs, whereas red points indicate identified compound extreme events.

Among the identified events, the most extreme corresponds to the Great Storm of October 16, 1987, combining an approximately 1200-year surge event with an 800-year river flow event. The resulting JRP of roughly 4500 years reflects the rarity of this compound occurrence. This storm affected large parts of Europe, producing exceptional surge levels and river flows. A second notable event occurred on October 30, 2000, with a JRP of about 90 years, combining a ~35-year surge event and a ~15-year river flow event. Additional illustrative scenarios are provided in Table S1.

The spatial analysis of compound flood impacts uses Aqueduct riverine flood maps and national NVE coastal flood maps (Table 1). A representative scenario (Figure S8) shows that riverine flooding covers a substantially larger area than coastal flooding, suggesting that riverine processes pose a broader spatial risk across Oslo. Nonetheless, coastal flooding, while more localized, affects densely populated waterfront zones. Areas near river mouths and low-lying coastal sections exhibit exposure to both flooding mechanisms, aligning with historical cases where riverine and coastal flooding co-occurred. These patterns reinforce the multivariate findings and highlight the spatially variable but interconnected nature of compound flood risk in Oslo.

3.2 | Extreme Rainfall and Landslides in Múlaþing

The preconditioned–triggering framework identifies instances in which extreme rainfall conditions precede landslides in Múlaþing. The baseline inventory includes several documented landslide events (Table S2), with daily joint extreme events accounting for the highest number of associated landslides, followed by 2-, 3-, and 5-day aggregated events. As daily data capture the strongest correspondence with observed landslides, subsequent analyses focus on daily rainfall and sNAPI combinations.

Not all historical landslides coincide with identified joint extreme rainfall–sNAPI events. Several cases involve limited rainfall or low antecedent moisture conditions—for example, the August 21, 2003 landslide occurred after only 5.8 mm of rainfall in 12 h. Similarly, some landslides occurred during intense rainfall but without elevated API values. In contrast, joint extreme rainfall–sNAPI conditions are more strongly linked to larger and more consequential landslide events, underscoring the importance of combined preconditioning and triggering mechanisms.

Figure 5 summarizes the extreme-event analysis. The 90th percentile is selected as the optimal threshold for both variables, corresponding to 27.1 mm rainfall and an sNAPI of 1.29 under baseline conditions, and 28.6 mm rainfall with an sNAPI of 1.93 for future projections. A total of 86 joint extreme events are identified during 1980–2016, increasing to 151 events in the future period (2030–2066), reflecting rising rainfall intensity and higher antecedent moisture under projected climate conditions.

In the baseline scenario, the largest daily rainfall event is 144.4 mm, corresponding to an RP of approximately 40 years. The

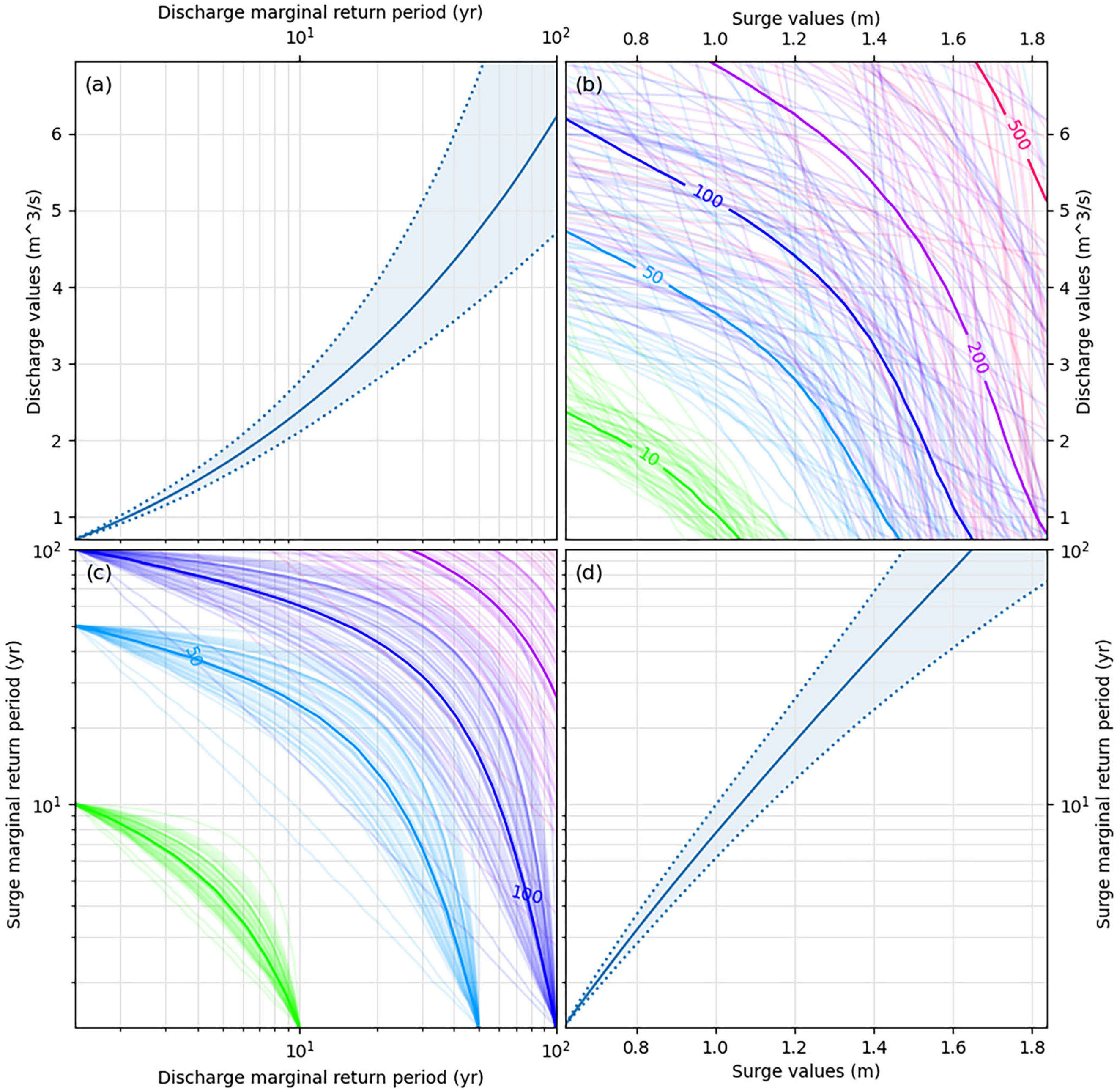

FIGURE 4 | Return period and joint-probability analyses for compound flooding in Oslo: (a and d) posterior marginal distributions for river discharge and surge levels across return periods (20th, 50th, and 80th percentiles); (b) JRPs across combinations of surge and discharge values; and (c) JRPs for selected joint extreme events. Contours represent JRPs (years), with bold lines indicating median estimates and lighter lines showing uncertainty from posterior samples.

maximum RP for sNAPI is around 160 years. The highest baseline JRP, about 200 years, results from the combination of a 2-year rainfall event and a 160-year sNAPI event. Under future climate conditions, maximum daily rainfall increases to 152.9 mm, but the highest JRP decreases substantially to roughly 25 years, associated with a 17-year rainfall event and an 18-year sNAPI event. Figures S9 and S10 illustrate these baseline and future results, whereas Figure 6 demonstrates that JRPs systematically decline in the future period across a wide range of rainfall–sNAPI combinations, indicating that extreme preconditioned–triggering sequences are expected to become more frequent.

The observed landslide inventory for Seyðisfjörður documents 44 landslides over 1980–2016, occurring on 18 distinct dates. The rainfall–sNAPI combinations identified in this study explain approximately 66% (n = 29) of these events. Table S3 provides return periods and intensities for each historical landslide. Landslides commonly occur in clusters affecting both northern and southern hillslopes simultaneously, driven by shared meteorological conditions. Heavy rainfall consistently appears as the predominant triggering factor in the historical record, reinforcing the relevance of the identified joint extreme rainfall–sNAPI thresholds.

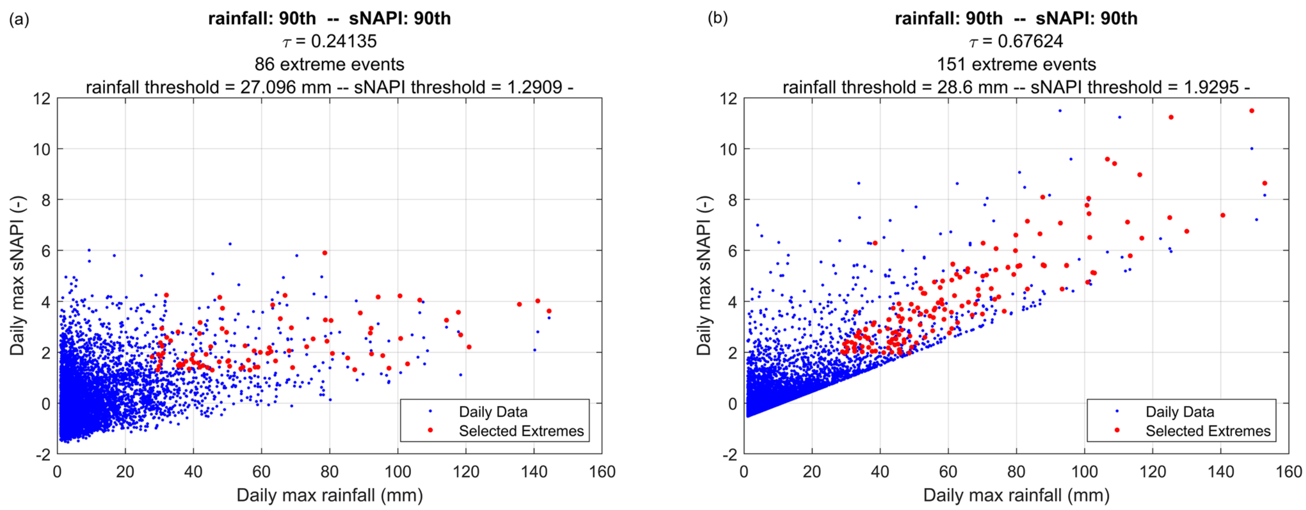

FIGURE 5 | Joint extreme rainfall and sNAPI events in Múlaþing, Iceland. Scatter plots of rainfall and sNAPI values, with blue points representing all observations and red points indicating joint extremes: (a) baseline conditions and (b) projected future climate scenario. sNAPI, scaled normalized antecedent precipitation index.

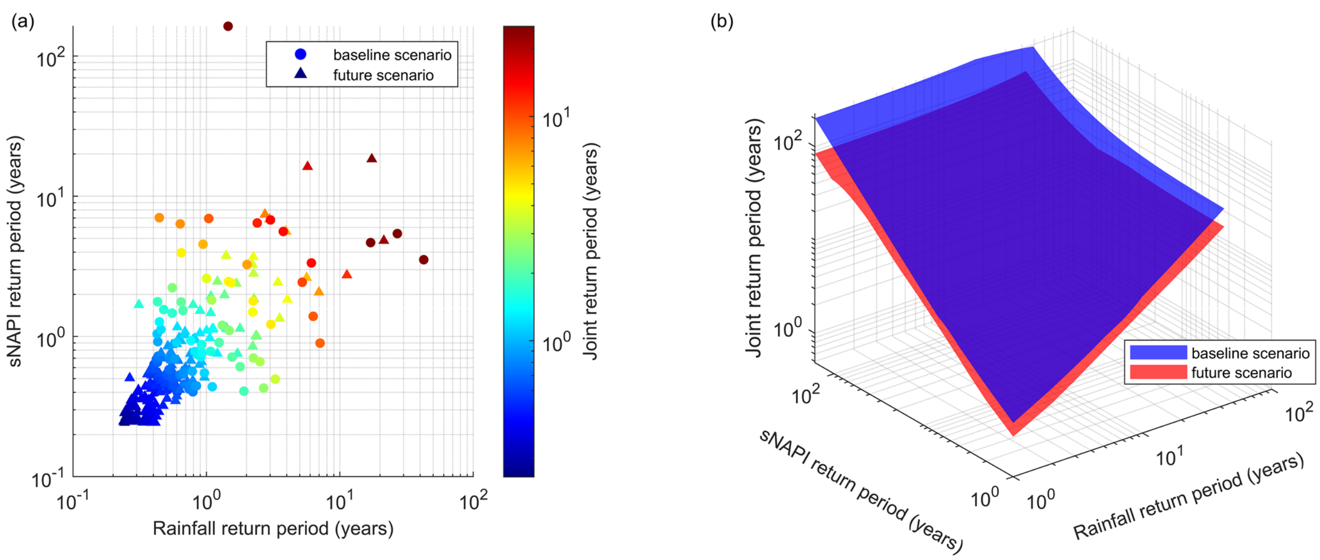

FIGURE 6 | JRPs of joint extreme rainfall and sNAPI extremes in Múlaþing, Iceland. (a) Estimated JRPs for identified joint extreme events under baseline and future scenarios. (b) Surface plot illustrating changes in JRPs between scenarios across different event combinations. sNAPI, scaled normalized antecedent precipitation index.

3.3 | Extreme Wind and Rainfall Events in Essex

Applying the spatially compounding framework to Essex identifies the 95th percentile of daily maximum wind speed and the 90th percentile of daily rainfall as the optimal thresholds, producing the highest Kendall's τ value of 0.16. These thresholds correspond to 12.65 m/s for wind speed and 13.86 mm for rainfall. Using these criteria, 34 joint extreme wind–rainfall events are detected during the baseline period (1981–2001), increasing to 47 events in the future period (2030–2050) (Figure 7).

During the baseline period, the strongest daily wind speed reaches 18.8 m/s—an event with an estimated RP of ~130 years—whereas the highest rainfall total (46.6 mm) corresponds to an RP of ~25 years. The most extreme joint event has a JRP of approximately 160 years, resulting from the combination of a 130-year wind event with a 2-year rainfall event. In the future scenario, both hazards intensify, with maximum RPs for wind and rainfall projected to increase substantially (to ~800 and ~1000 years, respectively). The most severe future joint event reaches a JRP of ~6400 years, reflecting the greater likelihood of co-occurring high wind and rainfall extremes under a warmer climate. A comparison of JRPs between baseline and future conditions is shown in Figure S18.

Spatial patterns of hazard intensities are assessed using the gridded data. Figure S19 illustrates 100-year extreme wind and rainfall events for both time periods. Results show an overall

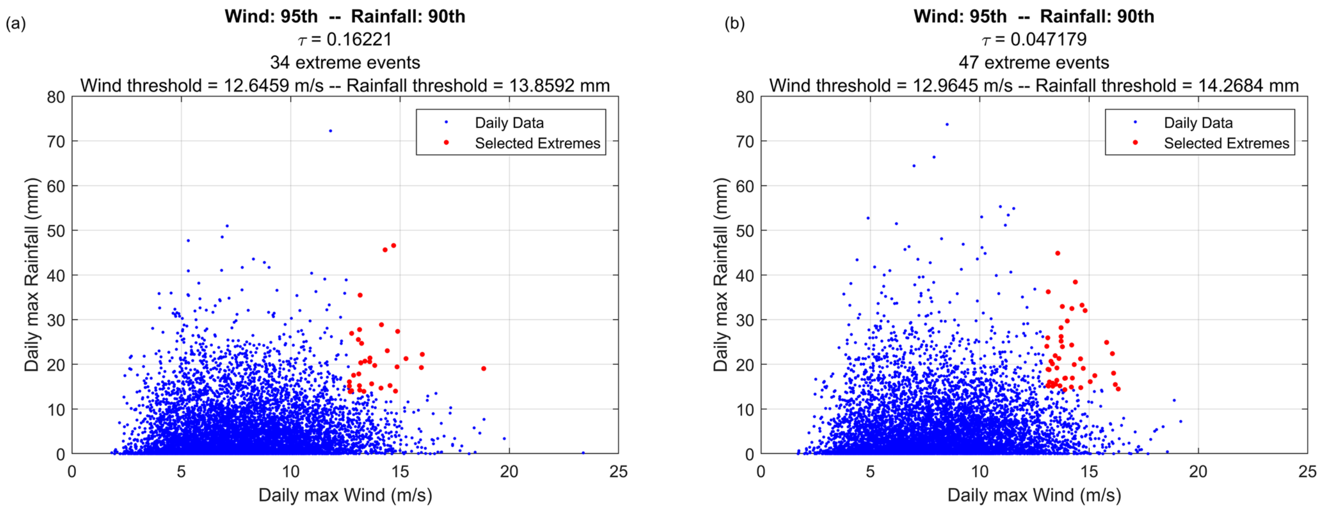

FIGURE 7 | Joint extreme wind and rainfall events in Essex, UK. Scatter plots of daily maximum wind speed and rainfall. Blue points represent all observations, and red points indicate joint extreme events. (a) Baseline conditions and (b) projected future scenario.

increase in hazard intensity by mid-century: Mean 100-year daily maximum wind speed rises from 10.7 (baseline) to 11.0 m/s (future), whereas mean 100-year rainfall increases from 20.2 to 21.2 mm. Coastal areas—already exposed to storm surges and high winds—experience the greatest intensification, and the geographic extent of areas affected by extreme wind and rainfall expands. Southwestern districts of Essex, in particular, are projected to face elevated exposure to spatially compounding hazards.

3.4 | Extreme Heat and Drought in Nice

The temporally compounding framework is used to assess the co-occurrence of extreme heat and drought in Nice. During the historical period, most of the region experiences at most 1 hot day per month. Under the high-emission scenario, however, the frequency of hot days increases substantially. In the near future, the French Mediterranean coast—including Nice—is projected to experience 2–4 hot days per month in June. By the end of the century, June is expected to feature 6–7 hot days, whereas July and August will see widespread intensification, with all areas experiencing at least 8 hot days in July and up to 11 in August. Figure S20 illustrates the spatial distribution of hot-day frequency across historical, near-future, and far-future periods, highlighting the expansion and intensification of heatwave conditions.

Drought patterns show contrasting temporal evolution. Historically, southern France exhibits slightly wet conditions, except in August when parts of Nice record negative SPI3 values. In the near future, mean SPI3 values indicate predominantly wet conditions across the domain. By the end of the century, however, August is projected to show widespread drying, with SPI3 values between −0.5 and −1 across much of the region. Figure S21 maps these changes, demonstrating a clear transition toward drier late-summer conditions under future climate scenarios.

Figure 8 presents the frequency of compound heatwave–drought events across the Nice domain. Historically, only small areas of southern France show ~4% compound-event frequency (equivalent to around 4 hot and dry months across the 30-year period), whereas Nice itself exhibits no compound events. In the near future, frequencies increase to approximately 3.5%–4% in parts of Nice. By the end of the century, compound-event frequencies exceed 10% across large parts of the region, indicating that some areas will experience at least 9 hot and dry summer months within the 30-year far-future period. These results demonstrate a pronounced escalation in compound heat–drought risk under continued high emissions.

4 | Discussion

4.1 | Contributions of the Generalized Multi-Hazard Framework

Quantifying multi-hazard interactions remains a major challenge due to the diverse ways in which hazards interact across temporal, spatial, and process dimensions. Existing approaches typically analyze multi-hazard events as simple compound or consecutive hazards, focus on specific hazard pairs, or rely on narrow temporal windows, limiting their applicability across different contexts (Bloomfield et al. 2024; Claassen et al. 2023; De Angeli et al. 2022). This study advances the field by proposing a generalized, process-informed framework that integrates four distinct categories of multi-hazard interactions—multivariate, preconditioned and triggering, spatially compounding, and temporally compounding events. Unlike previous approaches, which treat different types of multi-hazard interactions in an isolated way (Bevacqua et al. 2021), this framework explicitly analyzes interaction mechanisms between different types of multi-hazard events, analytical requirements, and relevant timescales, offering a more structured and comprehensive understanding of multi-hazard dynamics.

A key contribution lies in the integration of statistical, probabilistic, and geospatial methods within a unified system. The framework incorporates hazard-specific thresholds, optimized for the given datasets, informed by dependence metrics such as Kendall's τ, together with Bayesian copula models to quantify joint probabilities for short-term interactions. It also adapts

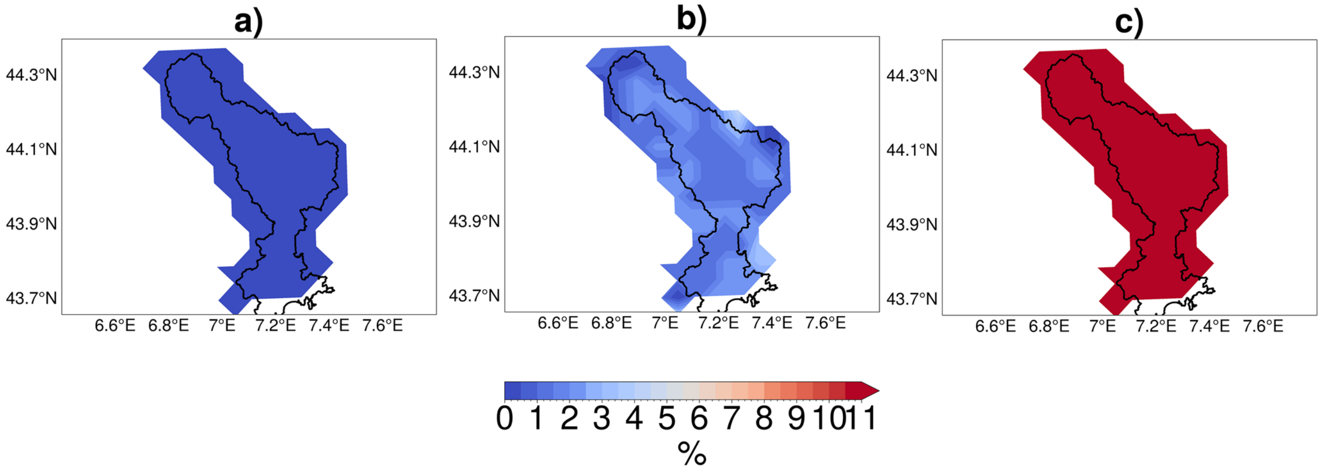

FIGURE 8 | Frequency of compound heatwave and drought events in Nice, France. Percentage occurrence of compound heatwave–drought events during summer for (a) historical period (1976–2005), (b) near future (2041–2070), and (c) far future (2071–2100).

temporal windows from hours to months and includes soil moisture proxies, rolling accumulations, and grid-based EVA to capture longer term or spatially distributed interactions. This dual statistical–geospatial design enables the framework not only to quantify probabilistic relationships between hazards but also to map the spatial distribution of hazard intensity and extent, addressing a gap in existing literature that often focuses solely on dependence estimation without translating results into spatially explicit hazard information (Bateni et al. 2022; Ghanbari et al. 2019, 2021). Furthermore, the framework is deliberately designed to be flexible and scalable, functioning across point-level observations, gridded climate simulations, and regional hazard fields. By formalizing differences in time (from 1-day to multi-month windows), space (single locations vs. regional domains), and scale (station data vs. gridded domains), it provides a robust structure that can be consistently applied to diverse hazard systems and regions. In doing so, it extends the conceptual models proposed in earlier work (Gill and Malamud 2014, 2016; Tilloy et al. 2019; Zscheischler et al. 2020) and operationalizes them in a manner that supports practical risk assessment, early-warning system enhancement, and climate adaptation planning. The flexibility of the framework enables its application to data-scarce settings, which is one of the major challenges in quantifying multi-hazard interrelationships (Thompson et al. 2025).

4.2 | Performance of the Framework Across the Four Case Study Regions

Application of the framework across four climatically and geographically distinct European regions demonstrates its adaptability, robustness, and practical relevance. In Oslo, for example, the multivariate analysis captures compound coastal–riverine flood interactions effectively. Dependence values are consistent with those reported in similar compound flood studies (Ghanbari et al. 2021; Ming et al. 2022), confirming the general applicability of the approach. The framework not only identifies historically significant events—such as the 1987 "Great Storm" (Engen 1988)—but also quantifies their rarity through JRPs and maps flood scenarios using available inundation datasets. This shows the framework's capability to detect extreme co-occurring hazards and translate joint-probability outputs into spatially meaningful insights, even in data-limited contexts.

In Múlaþing, the preconditioned and triggering component successfully captures the relationship between extreme rainfall, antecedent moisture (expressed through sNAPI), and landslide occurrence. Although not all landslides correspond to joint extreme rainfall–sNAPI events—owing to geomorphological or localized triggers—the framework explains approximately two-thirds of historical landslides in Seyðisfjörður. Its sensitivity to antecedent conditions is particularly valuable, as it identifies rainfall–moisture combinations that precede larger, more impactful events. Future projections suggest a doubling of such joint extremes, demonstrating how the framework can detect changes in hazard–precursor relationships under evolving climate conditions. In Essex, the spatially compounding framework identifies joint wind–rainfall extremes and highlights an increase in both frequency and intensity under future climate scenarios. The approach's ability to aggregate gridded datasets into spatially representative maxima, identify joint exceedances, and estimate JRPs allows for a nuanced understanding of how wind and rainfall interact over large spatial domains. Spatial results further reveal that future extremes affect a wider geographic area, with coastal and southwestern districts particularly exposed (Bloomfield et al. 2024), underscoring the framework's relevance for regional risk planning. Similarly, in Nice, the temporally compounding framework characterizes the co-occurrence of heatwaves and droughts at monthly timescales. Historical conditions show limited compound activity, yet both the occurrence and geographic extent of hot and dry summer months increase substantially under future high-emission scenarios. By the end of the century, parts of the region experience compound-event frequencies exceeding 10%, indicating that nearly 1 in every 10 summer months is projected to be both hot and dry. These findings align with broader evidence of Mediterranean climate intensification (Lee et al. 2024) and illustrate the ability of the framework to assess longer duration, climatological compound risks.

Across all four regions tested, the framework has been shown to adapt to different hazard drivers, data sources, temporal scales, and spatial configurations, providing consistent, structured insights into how hazard interactions emerge and evolve (Trogrlić et al. 2024). Nevertheless, uncertainties remain due to data limitations, secondary flood datasets, and climate-model variability. These challenges highlight the need for improved observational networks, enhanced climate projections, and integration of numerical hazard models to refine the assessment of multi-hazard characteristics, such as flood depth, velocity, and spatial dynamics. Despite these uncertainties, the framework demonstrates strong potential for operational multi-hazard risk assessment and serves as a useful tool for informing risk-informed decisions and climate resilience strategies.

5 | Conclusions

This study introduces a generalized, process-informed framework for assessing multi-hazard interactions across diverse temporal and spatial scales. By integrating statistical extreme-value methods, Bayesian dependence modeling, and geospatial analysis, the framework moves beyond conventional single-hazard approaches and provides a systematic means of characterizing multivariate, preconditioned and triggering, spatially compounding, and temporally compounding events. This integrated structure offers a novel contribution to multi-hazard research by explicitly differentiating hazard interaction types and tailoring analytical methods to their underlying physical processes.

Application of the framework to four European regions—Oslo, Múlaþing, Essex, and Nice—demonstrates its adaptability to varied climatic settings, data environments, and hazard combinations. Across these case studies, the framework reliably captures short-term joint extremes, identifies precursor–trigger relationships, characterizes spatially extensive hazard co-occurrence, and detects long-duration co-occurring climate anomalies. These results illustrate its effectiveness in revealing how interacting hazards evolve under present and future climate conditions, offering insights that can support more targeted and locally appropriate risk reduction strategies.

The growing interconnectedness and intensification of hazards under climate change underscores the need for frameworks capable of capturing cascading and compounding processes. The approach presented here helps clarify how such interactions shape impacts on people, infrastructure, and ecosystems, thereby strengthening the scientific foundations for climate resilience planning. It also supports the development of region-specific adaptation strategies aligned with international policy agendas, including the Sendai Framework, the Paris Agreement, and the EU Climate Adaptation Mission.

Future work should focus on integrating process-based numerical models, impact assessments, and socioeconomic dimensions into the framework to enhance predictive capability and strengthen links to decision-making. Such extensions would enable more detailed assessments of multi-hazard dynamics, particularly for complex flood processes and climate-driven hazard cascades. Overall, the framework provides a flexible and scalable tool for policymakers, planners, and risk managers seeking to build resilient and adaptive systems in the face of escalating multi-hazard risks.

Acknowledgments

This study was supported by the European Union's Horizon Europe project "Multi-hazard and Risk-Informed System for Enhanced Local and Regional Disaster Risk Management (MEDiate)" [grant agreement no. 101074075]. M.S.G.A. also received support from the Leverhulme Trust through an Early Career Fellowship [grant reference ECF-2023-074]. C.J.W. and E.T. acknowledge support from the European Union's Horizon Europe project "Towards enhanced coordination of disaster risk management and governance through a holistic framework for multi-level and cross-sectoral interaction and communication (TOGETHER)" [grant agreement 101226137], and C.J.W. also acknowledges support from the NERC Global Partnerships Seedcorn Fund "EMERGE" project [grant no. NE/W003775/1]. N.C.B. acknowledges support of the Italian inter-university PhD course in sustainable development and climate change (link: www.phd-sdc.it). M.A. and M.G. acknowledge support from the project "Dipartimento di Eccellenza 2023–2027," funded by the Italian Ministry of Education, University and Research at IUSS Pavia.

Conflicts of Interest

The authors declare no conflicts of interest.

Data Availability Statement

All data used in this analysis are from publicly available sources. The surge height and river flow data for Oslo, Norway, were obtained from the Norwegian Centre for Climate Services (https://seklima.met.no/observations/). Coastal flood maps for Oslo were sourced from The Norwegian Water Resources and Energy Directorate (NVE) at https://temakart.nve.no/. Riverine flood maps for Oslo were extracted from the Aqueduct Floods Hazard Maps provided by the World Resources Institute https://wri-projects.s3.amazonaws.com/AqueductFloodTool/download/v2/index.html. Extreme rainfall and landslide data for Múlaþing, Iceland, were obtained from the Icelandic Meteorological Office at https://en.vedur.is/. Modeled near-surface wind speed and rainfall data for Essex, UK, were acquired from EuroCORDEX-UK: Regional Climate Projections for the UK Domain https://catalogue.ceda.ac.uk/uuid/b109bd69e1af425aa0f661b01c40dc51/. Additionally, modeled temperature at 2 m and rainfall data for Nice, France, were sourced from EuroCORDEX: Regional Climate Simulations, Downscaled and Bias-Corrected Database, accessible at https://www.doi.org/10.24381/cds.9eed87d5. The MATLAB (MathWorks) toolbox, *detectExtremeEvents*, used for identifying joint extreme events, is available at the following GitHub repository: https://github.com/sarfarazadnan/detectExtremeEvents.git.

References

Arnalds, Þ., T. Jóhannesson, E. H. Jensen, and S. Sauermoser. 2002. *Hazard Zoning for Seyðisfjörður*. Veðurstofa Íslands.

Balkema, A. A., and L. De Haan. 1974. "Residual Life Time at Great Age." *Annals of Probability* 2: 792–804.

Barnes, C. 2023. *EuroCORDEX-UK: Regional Climate Projections for the UK Domain at 12 km Resolution for 1980–2080*. NERC EDS Centre for Environmental Data Analysis.

Bateni, M. M., M. L. Martina, and M. Arosio. 2022. "Multivariate Return Period for Different Types of Flooding in City of Monza, Italy." *Natural Hazards* 114: 811–823.

Berg, P., C. Photiadou, L. Simonsson, E. Sjokvist, J. Thuresson, and R. Mook. 2021. *Temperature and Precipitation Climate Impact Indicators From 1970 to 2100 Derived From European Climate Projections*. Copernicus Climate Change Service (C3S) Climate Data Store (CDS).

Bevacqua, E., C. De Michele, C. Manning, et al. 2021. "Guidelines for Studying Diverse Types of Compound Weather and Climate Events." *Earth's Future* 9: e2021EF002340.

Bevacqua, E., D. Maraun, M. I. Vousdoukas, et al. 2019. "Higher Probability of Compound Flooding From Precipitation and Storm Surge in Europe Under Anthropogenic Climate Change." *Science Advances* 5: eaaw5531.

Bloomfield, H., P. Bates, L. Shaffrey, et al. 2024. "Synoptic Conditions Conducive for Compound Wind-Flood Events in Great Britain in Present and Future Climates." *Environmental Research Letters* 19: 024019.

Boult, V. L., E. Black, H. Saado Abdillahi, et al. 2022. "Towards Drought Impact-Based Forecasting in a Multi-Hazard Context." *Climate Risk Management* 35: 100402.

Brunner, M. I., J. Seibert, and A. C. Favre. 2016. "Bivariate Return Periods and Their Importance for Flood Peak and Volume Estimation." *WIREs Water* 3: 819–833.

Carpenter, B., A. Gelman, M. D. Hoffman, et al. 2017. "Stan: A Probabilistic Programming Language." *Journal of Statistical Software* 76: 1–32.

Chen, H., S. Zhang, M. Peng, and L. M. Zhang. 2016. "A Physically-Based Multi-Hazard Risk Assessment Platform for Regional Rainfall-Induced Slope Failures and Debris Flows." *Engineering Geology* 203: 15–29.

Ciurean, R., J. Gill, H. Reeves, et al. 2018. *Review of Multi-Hazards Research and Risk Assessments*. Engineering Geology & Infrastructure Programme Open Report OR/18/057. British Geological Survey.

Claassen, J. N., P. J. Ward, J. Daniell, E. E. Koks, T. Tiggeloven, and M. C. de Ruiter. 2023. "A New Method to Compile Global Multi-Hazard Event Sets." *Scientific Reports* 13: 13808.

Cohen, S., G. R. Brakenridge, A. Kettner, et al. 2018. "Estimating Floodwater Depths From Flood Inundation Maps and Topography." *JAWRA Journal of the American Water Resources Association* 54: 847–858.

Coles, S., J. Bawa, L. Trenner, and P. Dorazio. 2001. *An Introduction to Statistical Modeling of Extreme Values*. Springer.

Cordery, I. 1970. "Initial Loss for Flood Estimation and Forecasting." *Journal of the Hydraulics Division* 96: 2447–2466.

De Angeli, S., B. D. Malamud, L. Rossi, F. E. Taylor, E. Trasforini, and R. Rudari. 2022. "A Multi-Hazard Framework for Spatial-Temporal Impact Analysis." *International Journal of Disaster Risk Reduction* 73: 102829.

De Ruiter, M. C., A. Couasnon, M. J. van den Homberg, J. E. Daniell, J. C. Gill, and P. J. Ward. 2020. "Why We Can no Longer Ignore Consecutive Disasters." *Earth's Future* 8: e2019EF001425.

Domeisen, D. I., E. A. Eltahir, E. M. Fischer, et al. 2023. "Prediction and Projection of Heatwaves." *Nature Reviews Earth & Environment* 4: 36–50.

Engen, I. 1988. *Flommen på Sør-og Østlandet i oktober 1987*. Norges Vassdrags og Energidirektorat, Publikasjon.

Fan, X., F. Yang, S. Siva Subramanian, et al. 2020. "Prediction of a Multi-Hazard Chain by an Integrated Numerical Simulation Approach: The Baige Landslide, Jinsha River, China." *Landslides* 17: 147–164.

Farahmand, A., and A. AghaKouchak. 2015. "A Generalized Framework for Deriving Nonparametric Standardized Drought Indicators." *Advances in Water Resources* 76: 140–145.

Fischer, E. M., and C. Schär. 2010. "Consistent Geographical Patterns of Changes in High-Impact European Heatwaves." *Nature Geoscience* 3: 398–403.

Ghanbari, M., M. Arabi, S. C. Kao, J. Obeysekera, and W. Sweet. 2021. "Climate Change and Changes in Compound Coastal-Riverine Flooding Hazard Along the U.S. Coasts." *Earth's Future* 9: e2021EF002055.

Ghanbari, M., M. Arabi, J. Obeysekera, and W. Sweet. 2019. "A Coherent Statistical Model for Coastal Flood Frequency Analysis Under Nonstationary Sea Level Conditions." *Earth's Future* 7: 162–177.

Ghosh, N. C., R. K. Jaiswal, and S. Ali. 2021. "Normalized Antecedent Precipitation Index Based Model for Prediction of Runoff From Un-Gauged Catchments." *Water Resources Management* 35: 1211–1230.

Gill, J. C., M. Duncan, R. Ciurean, et al. 2022. *MYRIAD-EU D1.2 Handbook of Multi-Hazard, Multi-Risk Definitions and Concepts. H2020 MYRIAD-EU Project, Grant Agreement Number 101003276*. British Geological Survey.

Gill, J. C., and B. D. Malamud. 2014. "Reviewing and Visualizing the Interactions of Natural Hazards." *Reviews of Geophysics* 52: 680–722.

Gill, J. C., and B. D. Malamud. 2016. "Hazard Interactions and Interaction Networks (Cascades) Within Multi-Hazard Methodologies." *Earth System Dynamics* 7: 659–679.

Gill, J. C., B. D. Malamud, E. M. Barillas, and A. Guerra Noriega. 2020. "Construction of Regional Multi-Hazard Interaction Frameworks, With an Application to Guatemala." *Natural Hazards and Earth System Sciences* 20: 149–180.

Gilleland, E., and R. W. Katz. 2016. "extRemes 2.0: an Extreme Value Analysis Package in R." *Journal of Statistical Software* 72: 1–39.

Gnyawali, K., K. Dahal, R. Talchabhadel, and S. Nirandjan. 2023. "Framework for Rainfall-Triggered Landslide-Prone Critical Infrastructure Zonation." *Science of the Total Environment* 872: 162242.

Gori, A., N. Lin, D. Xi, and K. Emanuel. 2022. "Tropical Cyclone Climatology Change Greatly Exacerbates US Extreme Rainfall–Surge Hazard." *Nature Climate Change* 12: 171–178.

Gringorten, I. I. 1963. "A Plotting Rule for Extreme Probability Paper." *Journal of Geophysical Research* 68: 813–814.

Gudendorf, G., and J. Segers. 2010. "Extreme-Value Copulas." In *Copula Theory and Its Applications: Proceedings of the Workshop Held in Warsaw, 25–26 September 2009*. Springer.

Gylfadóttir, S. S., T. Jóhannesson, J. K. Helgason, and M. H. Jónsson. 2021. *Endurskoðað Hættumat Fyrir Svæðið Frá Búðará Að Skuldarlæk Á Seyðisfirði (minnisblað)*. Icelandic Meteorological Office.

Han, L., J. Zhang, Y. Zhang, Q. Ma, S. Alu, and Q. Lang. 2019. "Hazard Assessment of Earthquake Disaster Chains Based on a Bayesian Network Model and ArcGIS." *ISPRS International Journal of Geo-Information* 8: 210.

Hao, Z., A. AghaKouchak, N. Nakhjiri, and A. Farahmand. 2014. "Global Integrated Drought Monitoring and Prediction System." *Scientific Data* 1: 1–10.

Hasan Tanim, A., and E. Goharian. 2021. "Developing a Hybrid Modeling and Multivariate Analysis Framework for Storm Surge and Runoff Interactions in Urban Coastal Flooding." *Journal of Hydrology* 595: 125670.

Hauser, M., L. Gudmundsson, R. Orth, et al. 2017. "Methods and Model Dependency of Extreme Event Attribution: The 2015 European Drought." *Earth's Future* 5: 1034–1043.

Heggen, R. J. 2001. "Normalized Antecedent Precipitation Index." *Journal of Hydrologic Engineering* 6: 377–381.

Hochrainer-Stigler, S., R. Šakić Trogrlić, K. Reiter, et al. 2023. "Toward a Framework for Systemic Multi-Hazard and Multi-Risk Assessment and Management." *Iscience* 26: 106736.

IPCC. 2013. *Climate Change 2013: The Physical Science Basis, Contribution of Working Group I to the Fifth Assessment Report of the Intergovernmental Panel on Climate Change (IPCC)*. IPCC.

Ismail, T., K. Ahmed, M. Alamgir, M. N. Kakar, and A. B. Fadzil. 2018. "Bivariate Flood Frequency Analysis Using Gumbel Copula." *Malaysian Journal of Civil Engineering* 30: 193–201.

Jensen, E., M. S. G. Adnan, E. Perugini, et al. 2024. *MEDiate: A Diagnosis and Assessment of the Primary Types of Interacting Hazards Related to European Areas: Deliverable D2.2*. European Commission.

Jensen, E., and T. Sönser. 2003. *Process Orientated Landslide Hazard Assessment for the South Side of Seyðisfjörður*. Veðurstofa Íslands.

Johnson, K., Y. Depietri, and M. Breil. 2016. "Multi-Hazard Risk Assessment of Two Hong Kong Districts." *International Journal of Disaster Risk Reduction* 19: 311–323.

Kendon, M., and M. McCarthy. 2015. “The UK’s Wet and Stormy Winter of 2013/2014.” *Weather* 70: 40–47.

Kennedy, C., J. Douglas, M. S. G. Adnan, et al. 2023. *A Generalised Framework for the Assessment of Current and Future Multi-Hazard Interactions, Multi-Hazard and Risk-Informed System for Enhanced Local and Regional Disaster Risk Management*. MEDiate.

Komendantova, N., F. Mulder, M. Danielson, et al. 2023. *Validation of the MEDiate Concept Model Through Literature and Workshops With Stakeholders From Testbeds*. MEDiate.

Latif, S., and F. Mustafa. 2020. “Bivariate Flood Distribution Analysis Under Parametric Copula Framework: A Case Study for Kelantan River Basin in Malaysia.” *Acta Geophysica* 68: 821–859.

Lee, R., C. J. White, M. S. G. Adnan, et al. 2024. “Reclassifying Historical Disasters: From Single to Multi-Hazards.” *Science of the Total Environment* 912: 169120.

Leonard, M., S. Westra, A. Phatak, et al. 2014. “A Compound Event Framework for Understanding Extreme Impacts.” *Wiley Interdisciplinary Reviews: Climate Change* 5: 113–128.

Li, X., Y. Wei, and F. Li. 2021. “Optimality of Antecedent Precipitation Index and Its Application.” *Journal of Hydrology* 595: 126027.

Liu, B., Y. L. Siu, and G. Mitchell. 2016. “Hazard Interaction Analysis for Multi-Hazard Risk Assessment: A Systematic Classification Based on Hazard-Forming Environment.” *Natural Hazards and Earth System Sciences* 16: 629–642.

Liu, X., N. Li, S. Yuan, N. Xu, W. Shi, and W. Chen. 2015. “The Joint Return Period Analysis of Natural Disasters Based on Monitoring and Statistical Modeling of Multidimensional Hazard Factors.” *Science of the Total Environment* 538: 724–732.

Massad, A., N. Petersen, T. Þórarinsdóttir, and M. Roberts. 2020. *Reassessment of Precipitation Return Levels in Iceland*. Vedurstofa Islands.

McKee, T. B., N. J. Doesken, and J. Kleist. 1993. “The Relationship of Drought Frequency and Duration to Time Scales.” In *Proceedings of the 8th Conference on Applied Climatology*. American Meteorological Society.

Ming, X., Q. Liang, R. Dawson, X. Xia, and J. Hou. 2022. “A Quantitative Multi-Hazard Risk Assessment Framework for Compound Flooding Considering Hazard Inter-Dependencies and Interactions.” *Journal of Hydrology* 607: 127477.

Ming, X., W. Xu, Y. Li, J. Du, B. Liu, and P. Shi. 2015. “Quantitative Multi-Hazard Risk Assessment With Vulnerability Surface and Hazard Joint Return Period.” *Stochastic Environmental Research and Risk Assessment* 29: 35–44.

Moftakhari, H. R., G. Salvadori, A. AghaKouchak, B. F. Sanders, and R. A. Matthew. 2017. “Compounding Effects of Sea Level Rise and Fluvial Flooding.” *Proceedings of the National Academy of Sciences* 114: 9785–9790.

Nawri, N., B. Pálmason, G. N. Petersen, H. Björnsson, and S. Þorsteinsson. 2017. *The ICRA Atmospheric Reanalysis Project for Iceland*. Icelandic Meteorological Office.

Ntegeka, V., P. Salamon, G. Gomes, et al. 2013. *EFAS-Meteo: A European Daily High-Resolution Gridded Meteorological Data Set for 1990–2011*. Report Eur 26408. Office of the European Union.

NVE. 2023. *The Norwegian Water Resources and Energy Directorate (NVE)*. NVE.

Park, M. H., and J. H. Kim. 2016. “Estimating Extreme Tail Risk Measures With Generalized Pareto Distribution.” *Computational Statistics & Data Analysis* 98: 91–104.

Perkins, S. E., and L. V. Alexander. 2013. “On the Measurement of Heat Waves.” *Journal of Climate* 26: 4500–4517.

Pickands, J. III 1975. “Statistical Inference Using Extreme Order Statistics.” *Annals of Statistics* 3: 119–131.

Pourghasemi, H. R., N. Kariminejad, M. Amiri, et al. 2020. “Assessing and Mapping Multi-Hazard Risk Susceptibility Using a Machine Learning Technique.” *Scientific Reports* 10: 3203.

Rebetez, M., H. Mayer, O. Dupont, et al. 2006. “Heat and Drought 2003 in Europe: A Climate Synthesis.” *Annals of Forest Science* 63: 569–577.

Rosendahl Appelquist, L., and K. Halsnæs. 2015. “The Coastal Hazard Wheel System for Coastal Multi-Hazard Assessment & Management in a Changing Climate.” *Journal of Coastal Conservation* 19: 157–179.

Rousi, E., K. Kornhuber, G. Beobide-Arsuaga, F. Luo, and D. Coumou. 2022. “Accelerated Western European Heatwave Trends Linked to More-Persistent Double Jets Over Eurasia.” *Nature Communications* 13: 3851.

Šakić Trogrlić, R., K. Reiter, R. L. Ciurean, et al. 2024. “Challenges in Assessing and Managing Multi-Hazard Risks: A European Stakeholders Perspective.” *Environmental Science & Policy* 157: 103774.

Salvadori, G., F. Durante, C. De Michele, M. Bernardi, and L. Petrella. 2016. “A Multivariate Copula-Based Framework for Dealing With Hazard Scenarios and Failure Probabilities.” *Water Resources Research* 52: 3701–3721.

Spencer, T., S. M. Brooks, B. R. Evans, J. A. Tempest, and I. Möller. 2015. “Southern North Sea Storm Surge Event of 5 December 2013: Water Levels, Waves and Coastal Impacts.” *Earth-Science Reviews* 146: 120–145.

Thompson, H. E., J. C. Gill, R. Šakić Trogrlić, F. E. Taylor, and B. D. Malamud. 2025. “A Methodology to Compile Multi-Hazard Interrelationships in a Data-Scarce Setting: An Application to the Kathmandu Valley, Nepal.” *Natural Hazards and Earth System Sciences* 25: 353–381.

Thompson, V., N. J. Dunstone, A. A. Scaife, et al. 2017. “High Risk of Unprecedented UK Rainfall in the Current Climate.” *Nature Communications* 8: 107.

Tilloy, A., B. D. Malamud, H. Winter, and A. Joly-Laugel. 2019. “A Review of Quantification Methodologies for Multi-Hazard Interrelationships.” *Earth-Science Reviews* 196: 102881.

van den Hurk, B., E. van Meijgaard, P. de Valk, K.-J. van Heeringen, and J. Gooijer. 2015. “Analysis of a Compounding Surge and Precipitation Event in the Netherlands.” *Environmental Research Letters* 10: 035001.

van Westen, C. 2012. *IncREO Increasing Resilience Through Earth Observation*. European Commission.

van Westen, C., and S. Greiving. 2017. “Multi-Hazard Risk Assessment and Decision Making.” In *Environmental Hazards Methodologies for Risk Assessment and Management*. IWA Publishing.

Wahl, T., S. Jain, J. Bender, S. D. Meyers, and M. E. Luther. 2015. “Increasing Risk of Compound Flooding From Storm Surge and Rainfall for Major US Cities.” *Nature Climate Change* 5: 1093–1097.

Wang, J., X. Gu, and T. Huang. 2013. “Using Bayesian Networks in Analyzing Powerful Earthquake Disaster Chains.” *Natural Hazards* 68: 509–527.

Ward, P. J., J. Daniell, M. Duncan, et al. 2022. “Invited Perspectives: A Research Agenda Towards Disaster Risk Management Pathways in Multi-(Hazard-) Risk Assessment.” *Natural Hazards and Earth System Sciences* 22: 1487–1497.

Ward, P. J., H. C. Winsemius, S. Kuzma, et al. 2020. *Aqueduct Floods Methodology*. World Resources Institute.

Wu, J., H. Yao, X. Chen, G. Wang, X. Bai, and D. Zhang. 2022. “A Framework for Assessing Compound Drought Events From a Drought Propagation Perspective.” *Journal of Hydrology* 604: 127228.

Xi, D., N. Lin, and A. Gori. 2023. “Increasing Sequential Tropical Cyclone Hazards Along the US East and Gulf Coasts.” *Nature Climate Change* 13: 258–265.

Xie, W.-P., and J.-S. Yang. 2013. “Assessment of Soil Water Content in Field With Antecedent Precipitation Index and Groundwater Depth in the Yangtze River Estuary.” *Journal of Integrative Agriculture* 12: 711–722.

Zhao, Y., F. Wei, H. Yang, and Y. Jiang. 2011. “Discussion on Using Antecedent Precipitation Index to Supplement Relative Soil Moisture Data Series.” *Procedia Environmental Sciences* 10: 1489–1495.

Zscheischler, J., O. Martius, S. Westra, et al. 2020. "A Typology of Compound Weather and Climate Events." *Nature Reviews Earth & Environment* 1: 333–347.

Zscheischler, J., and S. I. Seneviratne. 2017. "Dependence of Drivers Affects Risks Associated With Compound Events." *Science Advances* 3: e1700263.

Supporting Information

Additional supporting information can be found online in the Supporting Information section.

Supplementary Material: cli270063-sup-0001-SuppMat.docx